On the Chemical State and Distribution of Zr- and V-based Additives in Reactive Hydride Composites

U Bösenberg[1], U Vainio[2], P K Pranzas[1], J M Bellosta von Colbe[1], G Goerigk[3], E Welter[2], M Dornheim[1], A Schreyer[1], R Bormann[1]

[1] Institute of Materials Research, GKSS Research Centre Geesthacht, Max-Planck-Str.1, D-21502 Geesthacht, Germany
[2] HASYLAB at Deutsches Elektronen-Synchrotron A Research Centre of the Helmholtz Association, Notkestrasse 85, D-22607 Hamburg, Germany
[3] Institut für Festkörperforschung, Forschungszentrum Jülich, Leo-Brandt-Str., D-52425 Jülich, Germany

E-mail: ulrike.boesenberg@gkss.de

Abstract. Reactive hydride composites (RHCs) are very promising hydrogen storage materials for future applications due to their reduced reaction enthalpies and high gravimetric capacities. At present, the materials functionality is limited by the reaction kinetics. A significant positive influence can be observed with addition of transition-metal-based additives. To understand the effect of these additives, the chemical state and changes during the reaction as well as the microstructural distribution were investigated using X-ray absorption near edge structure (XANES) spectroscopy and anomalous small-angle X-ray scattering (ASAXS). In this work, zirconium- and vanadium-based additives were added to $2\,LiBH_4$ - MgH_2 composites and $2\,LiH$ - MgB_2 composites and measured in the vicinity of the corresponding absorption edge. The measurements reveal the formation of finely distributed zirconium-diboride and vanadium-based nanoparticles. The potential mechanisms for the observed influence on reaction kinetics are discussed.

PACS numbers: 81.07.Bc, 82.30.RS, 61.05.cf

1. Introduction

Hydrogen is one of the favored energy carriers for the future. To make mobile application possible, a reliable storage solution has to be developed. From the safety point of view, one very promising option is the chemical storage in solid state metal compounds, metal hydrides. For application, high gravimetric storage capacities coupled with suitable desorption temperatures need to be mastered. From the thermodynamic point of view, no single, pure metal or complex hydride fulfills the requirements concerning reaction enthalpies and desorption temperature simultaneously. Alloying or the formation of intermetallic compounds is a well known method of thermodynamic tuning since the pioneering work of Libowitz *et al* [1]. Trying to destabilize MgH_2 Reilly and Wiswall [2; 3] have been the first, who, by adding $MgCu_2$ to MgH_2 discovered that reaction enthalpies can be decreased by additives which react exothermically with the hydride during desorption. These approaches are usually accompanied by a significant decrease in the gravimetric capacity of the hydride due to the combination with heavier metal elements like, e.g., copper or nickel. To overcome this drawback, recently the Reactive Hydride Composites (RHC) were developed [4; 5; 6; 7]. In these a chemical reaction between two or more hydrides lowers the overall reaction enthalpy while the gravimetric hydrogen storage capacity remains high. In the present work, the focus is put on the $2\,LiBH_4$ - MgH_2 composites forming $2\,LiH$ - MgB_2 composites in the desorbed state. This system shows a reversible hydrogen capacity of approximately 10.5 wt% and a theoretically assessed reaction enthalpy of 46 kJ/mol H_2, leading to an estimated equilibrium temperature of 170 °C at 1 bar H_2. However, at present the desorption occurs in a two-step reaction mechanism and takes only place at elevated temperatures with slow kinetics [8; 9; 10; 11]. A significant improvement can be observed upon the addition of transition-metal based additives. This is not a surprising observation, because for the well known light metal hydrides MgH_2 and $NaAlH_4$ transition-metal based additives play a crucial role in the reaction kinetics and reversibility, see e.g. [12; 13]. However, it should be noted that in case of $NaAlH_4$ the mechanism is not fully understood yet.

So far, the description of effect of the additives in RHCs has been mainly phenomenological in terms of the reaction kinetics. To understand the underlying mechanism, a knowledge of the chemical state and the microstructural distribution is necessary. The herein added vanadium-chloride (VCl_3), zirconium-chloride ($ZrCl_4$) and zirconium-isopropoxide isopropanol (Zr-iso) are highly reactive, reactions during the high-energy ball milling process for materials preparation are likely and a change in the chemical state is therefore probable. For application, not only is the chemical state after synthesis important but also the evolution during the cycling and the stability. In the present study, the chemical state of the zirconium-based additives has been investigated by X-ray absorption near edge structure spectroscopy (XANES) after synthesis and after the first and the second sorption reaction. From this analysis, conclusions on the local structure around the atoms of a selected element like the valence state and the

local symmetry and therefore on the bonding are drawn by comparison with reference materials.

Besides the chemical state, the microstructural distribution of the reacting phases as well as of the additive phase plays an important role in the sorption kinetics. Many common techniques such as, e.g., electron microscopy cannot be applied or only under certain precautions, because the materials react readily with air. Furthermore, they are only partially stable under the electron beam, display poor conductivity and the light elements such as hydrogen, lithium and boron cannot be detected by standard techniques such as energy dispersive X-ray spectroscopy (EDX). High resolution must be reached to characterize the fine microstructure of the nanocrystalline composites. Nevertheless, such studies are possible, and first TEM investigations on the currently investigated RHC with titanium-based additives display a uniform distribution of titanium in the sample down to an observed size scale of approximately 200 nm [14]. This indicates a very fine additive distribution and sizes much smaller than 200 nm for the corresponding additive phase. But high or atomic resolution has not yet been achieved for these compounds and therefore information on the local structure and chemical state was not obtained.

To characterize the nanostructure of a material, small-angle scattering (SAS) using neutrons (SANS) or photons (SAXS) is a well known tool, giving also the advantage to average over the whole sample rather than probing locally. The intensity of the scattered radiation at angles below 5° is recorded to analyze structures in the range of typically 0.5-100 nm and can be applied for samples with different structure, such as solid, liquid or amorphous. In anomalous small-angle X-ray scattering (ASAXS) the change in the complex scattering factors at the absorption edge of the respective element leads to a change in the scattered intensity as a function of energy. By measuring at several energies in the vicinity of the absorption edge, the scattering contribution from the respective element (i.e. V or Zr) containing structures can be separated from the total scattering coming from the material [15]. The absorption edges of metallic Zr and V are at 17998 eV and 5465 eV, respectively.

The present study gives the first insight into the chemical state and distribution of V- and Zr-based additives in reactive hydride composites and contributes to the understanding of the mechanism by which transition metal based additives influence sorption kinetics.

2. Experimental

2.1. Sample preparation

All samples were prepared by high energy ball milling in a Spex 8000 Mixer Mill, using a ball to powder ratio of 10:1 and a milling time of 5 hours. The initial microcrystalline powders $LiBH_4$ (95 % purity), LiH (99.4 % purity), MgB_2, VCl_3, $ZrCl_4$ and Zr-isopropoxide isopropanol complex (Zr-iso) were purchased from Alfa Aesar.

MgH_2 (98 % purity the rest being Mg) was obtained from Goldschmidt. 10 mol% additive was added to the initial mixture of $2\,LiH + MgB_2$. For the initial $2\,LiBH_4$-MgH_2 composites, the MgH_2 was pre-milled for 5 hours before the $LiBH_4$ and 10 mol% additive were added. The comparatively large amount of additive ensured a good contrast during the measurements.

To obtain the different sorption states, cycling was performed in a Sievert's type apparatus, designed by HERA Hydrogen Systems, Hydro Quebec, employing 5 bar hydrogen back pressure for the desorption reaction at a constant temperature of 400 °C. Absorption was performed under 30 or 50 bar hydrogen at 350 °C. The same materials were used for the ASAXS and the XANES measurements with approximately four weeks between the experiments.

All preparation and handling of the materials was performed in continuously purified argon atmosphere in a glovebox.

2.2. X-ray absorption near edge structure (XANES)

XANES measurements were only performed on the Zr-containing samples up to now. The samples were mixed with cellulose and pressed into pellets of 11 mm in diameter. These pellets were mounted between two 55 µm Kapton tapes on aluminum sample holders. The samples were then measured 3 times for approximately one hour in the energy range of 17200 to 19000 eV under vacuum conditions at beamline A1, Hasylab, DESY [16; 17].

2.3. Anomalous small-angle X-ray scattering (ASAXS)

For ASAXS measurements, the Zr-containing powders were filled in 1 mm thick sample holders of aluminum with a hole of 5 mm in diameter and sealed by two 55 µm thick Kapton tapes in an argon filled glovebox. To reach similar transmission values, the thickness for the V-containing samples had to be reduced to approximately 50 µm. The measurements were performed under vacuum conditions at beamline B1, Hasylab, DESY [18; 19]. Prior to each ASAXS measurement, a low resolution XANES scan was measured to determine the position of the absorption edge of each sample. For the Zr-containing samples, the energy of radiation was tuned across the K-absorption edge of Zr at 17998 eV in steps of 1 eV and similarly for the V-containing samples around 5465 eV. The flux of the direct beam and that of the beam transmitted by the sample was measured with a photodiode. The ASAXS intensities were measured at 5 or 6 energies below the previously determined absorption edges for the Zr-containing materials and at 3 energies for the V-containing samples. The sample-to-detector distances were 935 mm and 3635 mm. q is defined as the magnitude of the scattering vector with $q = 4\pi \sin\theta/\lambda$, where 2θ is the scattering angle and λ the wavelength. The reliable q range of the instrument in the energy range of Zr was concluded to be from 0.2 to 14 nm^{-1} and in the energy range of V from 0.1 to 4 nm^{-1}. Three measurement cycles were performed for each sample at each energy and distance. The measured 2D data was corrected for dark

current, detector response, transmission of the sample, and for geometrical distortion and integrated azimuthally. Further, the intensity was put on an absolute intensity scale by using pre-calibrated glassy carbon standards. A q^{-4} dependence was fitted to the scattering data at high q values and the determined constant is then subtracted to correct the data for an energy dependent background due to resonant Raman scattering and fluorescence.

Due to the large electron density contrast between zirconium or vanadium and the hydride matrix the materials are treated as two-phase systems. The X-ray scattering intensity $I(q)$ can then be written as [20]

$$\begin{aligned} I(q,E) = & x_\alpha \left| f_\alpha(q,E) \right|^2 S_{\alpha\alpha}(q) \\ & + 2x_\beta \Re \left[f_\alpha(q,E) f_\beta(q,E) \right] S_{\alpha\beta}(q) \\ & + x_\beta \left| f_\beta(q,E) \right|^2 S_{\beta\beta}(q) \end{aligned} \tag{1}$$

where $f(q,E) = f_0 + f'(q,E) + if''(q,E)$ is the atomic scattering factor, where $f_0 = Z$, the number of electrons (atomic number) and $f'(q,E)$, $f''(q,E)$ are the so called anomalous dispersion corrections. The dependence of f on q is small for small angles and is here neglected. x_α and x_β correspond to the atomic fractions of the two phases α and β, S are the partial structure factors (PSFs). Only the real part $\Re$ of the cross term contributes to the scattering intensity because the imaginary parts cancel each other out for $S_{12} = S_{21}$. The PSF for zirconium $S_{\beta\beta}$ could not be solved reliably from equation 1 nor by using the derivative method described in [21], because no stable solution could be obtained. However, the scattering contribution from the cross term $S_{\alpha\beta}(q)$ was assessed to be small within the resolved q-range and it was therefore neglected for the further analysis. Then the difference between two intensities measured at two energies gives the PSF for zirconium. The change in f' between the two energies was about 5.3. The anomalous dispersion corrections, f' and f'' were obtained from the XANES measurements using the CHOOCH program [22; 23], and are tabulated with the corresponding energies in table 1. The edge position for each sample was determined experimentally from the XANES measurements at beamline A1 by determination of the first inflection point of the derivative as described in [24].

To analyze the size distribution of the Zr-containing compounds, the Debye-Bueche model was used. It is a simple two phase model with sharp interfaces but random shape and distribution of the phase. Debye [25] first developed and applied the model, and recently it was applied by Goerigk and Williamson [26; 27] on ASAXS data. The separated scattering curves were fitted by the following model function.

$$I(q) = \frac{ba^3}{(1+a^2q^2)^2} + \frac{c}{q^4} \tag{2}$$

with the correlation length a, from which the two correlations lengths of the phases α and β, ξ_α and ξ_β, are calculated according to $1/a = 1/\xi_\alpha + 1/\xi_\beta$ and $\xi_\beta = a/(1-\Phi_\beta)$. Φ_β corresponds to the volume fraction of the Zr-containing phase β. Constant b includes information on volume fraction, density and concentration of phase β. However, the

Table 1. Anomalous dispersion corrections obtained from the XANES measurements at Beamline A1 for each applied energy and the experimentally determined absorption edge position for each sample.

Sample	ASAXS Energies (eV)	f'	f"	Edge Energy (eV)
$2\,LiBH_4 + MgH_2 + 0.1ZrCl_4$-milled	17645	-3.05	0.56	18007
	18003	-7.63	1.91	
$2\,LiBH_4 + MgH_2 + 0.1ZrCl_4$-desorbed	17645	-3.05	0.56	18008
	18006	-7.78	2.5	
$2\,LiBH_4 + MgH_2 + 0.1ZrCl_4$-absorbed	17645	-3.05	0.56	18008
	18006	-7.84	2.47	
$2\,LiBH_4 + MgH_2 +$ 0.1 Zr-iso-milled	17641	-3.02	0.56	18012
	18001	-7.05	1.02	
$2\,LiBH_4 + MgH_2 +$ 0.1 Zr-iso-desorbed	17641	-3.04	0.56	18009
	18001	-7.51	1.48	
$2\,LiBH_4 + MgH_2 +$ 0.1 Zr-iso-absorbed	17641	-3.04	0.56	18009
	18001	-7.51	1.46	
$2\,LiH + MgB_2 + 0.1ZrCl_4$-milled	17648	-3.03	0.54	18006
	18003	-7.25	1.8	
$2\,LiH + MgB_2 + 0.1ZrCl_4$-desorbed	17645	-3.02	0.54	18009
	18006	-7.65	2.32	
$2\,LiH + MgB_2 + 0.1ZrCl_4$-absorbed	17645	-3.02	0.54	18009
	18006	-7.63	2.22	
$2\,LiH + MgB_2 +$ 0.1 Zr-iso-milled	17641	-2.99	0.51	18013
	18001	-6.29	0.96	
$2\,LiH + MgB_2 +$ 0.1 Zr-iso-desorbed	17641	-3.04	0.56	18009
	18001	-7.36	1.29	
$2\,LiH + MgB_2 +$ 0.1 Zr-iso-absorbed	17645	-3.05	0.56	18007
	18006	-7.76	2.48	18014
Zr-powder				17998
ZrB_2				18008
$ZrCl_4$				18009
Zr-iso				18012

equations described in [27] cannot be solved for b in this case, because the density of the material and, due to the ongoing chemical reactions, exact composition is not known. Therefore the volume fractions were estimated from the chemical formula of the composites. The additional c/q^4-term takes large Zr-containing inhomogeneities into account; c is a constant.

3. Results

In figure 1 the kinetic behavior of the desorption reactions, obtained by volumetric measurements, are shown. As Zr is a heavy element and due to possible reactions, the storage capacities are drastically reduced to approximately 5.5 wt% in case of the samples with 10 mol% Zr-iso and 7.5 wt% for the 10 mol % $ZrCl_4$ containing samples. For better comparison, the reactions are normalized in the graphic. The materials were measured under a back pressure of 5 bar H_2 and isothermal conditions of 400 °C. Under these conditions a two step reaction is observed. The pure composite suffers from severe kinetic constraints with a lengthy incubation period between the two desorption steps. The impact of the additives especially on the incubation period is significant. Furthermore, there is also an impact on the reaction rates for the second step of the

reaction, where Zr-iso reveals the highest reaction rates. In case of the $ZrCl_4$ containing sample, the reaction rate for the second step decelerates during desorption. This beneficial effect of the additives is sustainable also for further sorption reactions leading to similar kinetics. The possible origin of the effect will be discussed below.

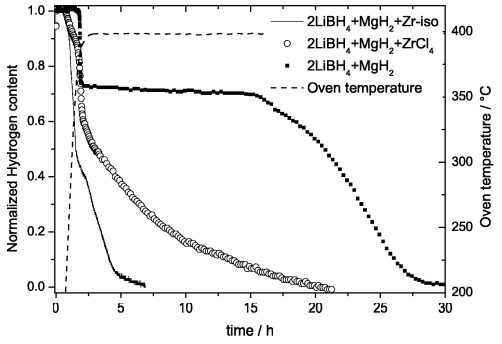

Figure 1. Volumetric measurements of the first desorption reaction of 2 $LiBH_4$ - MgH_2 composites with 10 mol% $ZrCl_4$ or Zr-iso compared to the material without additives measured under 5 bar hydrogen back pressure.

XANES data of the reference samples, and milled and cycled samples are shown in figure 2. For this data, the initial intensities from the three measurement cycles were added, the sloped background before the edge subtracted and then normalized to the value at 18100 eV. As reference materials Zr-metal, ZrO_2, ZrB_2 and the initial additives Zr-isopropoxide-isopropanol (Zr-iso) and $ZrCl_4$ were measured.

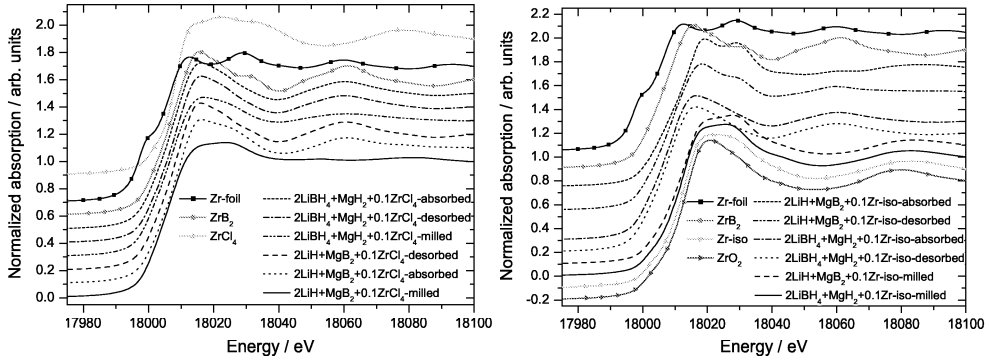

(a) $ZrCl_4$ (b) Zr-iso

Figure 2. XANES curves of the samples with the respective additives. The curves are shifted vertically for better visualisation.

The curves obtained for the materials prepared with additional $ZrCl_4$ show little similarity to the initial absorption edge of $ZrCl_4$. In these samples the position of the edge was the same; see table 1 for comparison. There are some variations in the amplitude of the oscillations in the post-edge region. They are probably due to the nanocrystalline state of the compound. The materials are apparently reduced during

the milling, however not to metallic Zr, because the absorption edge is slightly shifted to lower energies but not to the value of metallic Zr. The state is stable upon further cycling. For these samples, the formation of ZrB_2 is proposed. This is illustrated in figure 3 by the difference curves of milled and cycled $2\,LiBH_4 + MgH_2 + 0.1ZrCl_4$ composites to $ZrCl_4$ and ZrB_2. The XANES results of all $ZrCl_4$ containing samples show a very high similarity to those obtained for pure ZrB_2 and significant differences to the initial $ZrCl_4$.

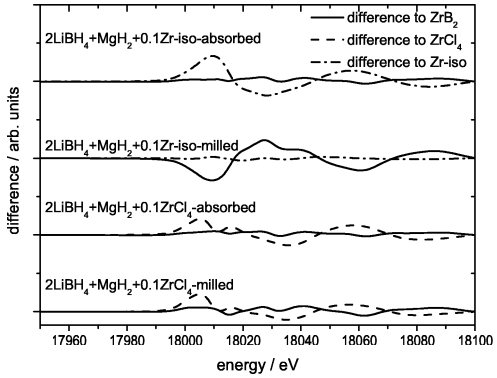

Figure 3. Difference curves of the XANES measurements for four selected samples to $ZrCB_2$, Zr-iso or $ZrCl_4$.

The matter is more difficult for the materials prepared with additional Zr-iso. Upon milling, there seem to be no changes in the chemical state, which is also confirmed by the Bragg peaks of Zr-iso measured in the ASAXS measurements and the similarity to the initial Zr-iso in figure 3 of the $2\,LiBH_4 + MgH_2 + 0.1$ Zr-iso composites. After the first sorption reaction, the Zr is reduced to a lower valency state, indicated by a shift of the absorption edge to lower energy, see table 1. Also the bonding has changed as indicated by the post-edge peak positions. For example, in the region of 18060 eV, the milled samples display a minimum, whereas after the first cycle a maximum is displayed. Investigations by other methods such as in-situ X-ray diffraction as well as differential scanning calorimetry indicate a reaction with the composite around 300 °C during the first heating. Formation of a ZrB_2 phase then is likely. ZrB_2 is observed for the cycled samples of initial $2\,LiBH_4 + MgH_2 + 0.1$ Zr-iso composites, in figure 3 the difference curve to ZrB_2 is almost zero. In the first sorption reactions in $2\,LiH + MgB_2$ +0.1 Zr-iso composites, the Zr is slightly reduced but the edge position has not reached the typical edge position for ZrB_2. A stable state is not reached and a mixture of different chemical states of Zr is likely after one sorption cycle for these composites. The details of the chemical state of the additives such as Zr- as well as Ti- and V-based additives by X-ray absorption spectroscopy are subject of further study.

In figure 4, the original scattering curves for all energies are shown exemplarily for the sample $2\,LiBH_4 + MgH_2 + 0.1$ $ZrCl_4$-milled. The shift of the intensity to lower values with increasing energy is significant. The broad peak at approximately $4\,nm^{-1}$ is caused by the Kapton tape of the sample holder. The high scattering cross section at

high q values for the measurements at the higher energies are due to resonant Raman scattering and fluorescence. This constant background was subtracted prior to further analysis.

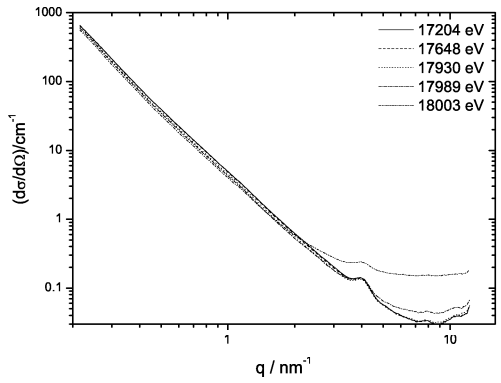

Figure 4. SAXS data for the sample $2\,LiBH_4 + MgH_2 + 0.1ZrCl_4$-milled obtained at 17200, 17648, 17930, 17989 and 18003 eV.

The obtained separated curves from the ASAXS measurements are shown for all samples in figure 5, where the symbols present the experimental data and the lines the fits according to equation (2). The fitted correlation lengths are listed in table 2. In combination with the estimated volume fraction for ZrB_2 the characteristic length of the ZrB_2 (ξ_β) and of the hydride matrix (ξ_α) are calculated. However, the value of the volume fraction is not known exactly, as the chemical state is assumed to be homogeneous in the sample and the density of the bulk materials is considered and the porosity neglected in the calculations. Therefore the matrix-length ξ_α can only serve as an estimate. However, it matches nicely the estimated crystallite sizes.

The milled composites with additional Zr-iso reveal no structures in the measured size range of approximately 0.4 to 30 nm and show only scattering from larger structures. The peak at $7\,nm^{-1}$ is a Bragg peak attributed to the Zr-iso in the milled composite. The lack of small structures is therefore reasonable. Upon cycling, distinct changes become noticeable. For the materials with additional Zr-iso a hump at approximately $2\,nm^{-1}$ forms and becomes more pronounced with cycling. This corresponds to structures with a size of around 1 nm. These observations can not be translated directly to materials with additional $ZrCl_4$. In the latter case stable ZrB_2 nanoparticles seem to have formed during milling. The associated correlation lengths are approximately 1 to 2 nm. They remain almost constant upon further cycling. For the $LiH - MgB_2$ composites with additional $ZrCl_4$, an additional formation of larger inhomogeneities can be observed due to the increased scattering in the small q-region.

Due to poor detector sensitivity at the low energies in case of the V-containing samples (5465 eV), only the scattering results from the sample set of $2\,LiH + MgB_2 + 0.1VCl_3$ could be reliably analyzed. For these samples, very similar results were obtained. The results for $2\,LiH + MgB_2 + 0.1VCl_3$ composites in different cycling states are shown in figure 6.

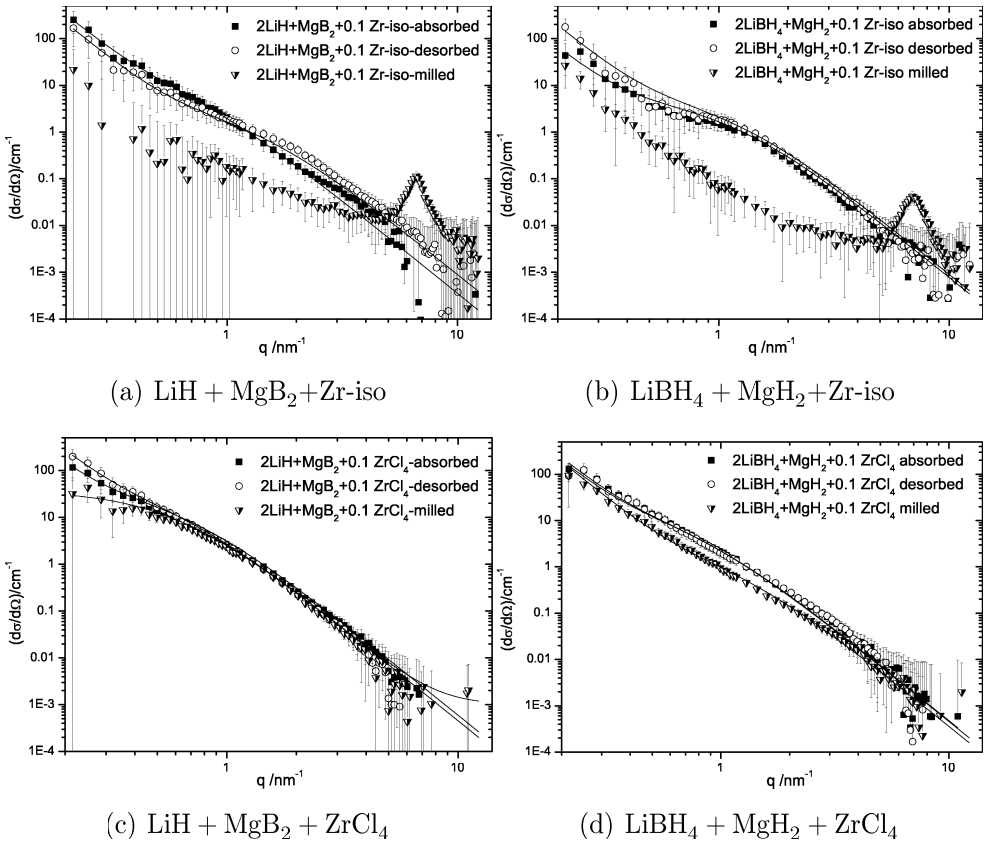

(a) $LiH + MgB_2$+Zr-iso (b) $LiBH_4 + MgH_2$+Zr-iso

(c) $LiH + MgB_2 + ZrCl_4$ (d) $LiBH_4 + MgH_2 + ZrCl_4$

Figure 5. Separated scattering curves for the as prepared and cycled composites obtained from ASAXS measurements at the K absorption edge of Zr at 17998 eV. The symbols represent the measured data whereas the lines correspond to the obtained fit applying the Debye-Bueche model described by equation (2).

Table 2. Characteristic length obtained by fitting with the Debye-Bueche model.

Sample	correlation length a (nm)	Volume fraction Φ_β	ξ_β (nm)	ξ_α (nm)
$2\,LiBH_4 + MgH_2 + 0{\cdot}1\,ZrCl_4$-absorbed	1.4	0.023	1.4	60.9
$2\,LiBH_4 + MgH_2 + 0{\cdot}1\,ZrCl_4$-desorbed	1.4	0.04	1.4	35.0
$2\,LiBH_4 + MgH_2 + 0{\cdot}1\,ZrCl_4$-milled	0.9	0.023	0.9	39.1
$2\,LiBH_4 + MgH_2 + 0{\cdot}1\,Zr-$iso-absorbed	0.9	0.03	0.9	30.0
$2\,LiBH_4 + MgH_2 + 0{\cdot}1\,Zr-$iso-desorbed	0.9	0.03	0.9	30.0
$2\,LiH + MgB_2 + 0{\cdot}1\,ZrCl_4$-absorbed	1.6	0.023	1.6	69.6
$2\,LiH + MgB_2 + 0{\cdot}1\,ZrCl_4$-desorbed	1.7	0.04	1.8	42.5
$2\,LiH + MgB_2 + 0{\cdot}1\,ZrCl_4$-milled	1.8	0.04	1.9	45.0
$2\,LiH + MgB_2 + 0{\cdot}1\,Zr-$iso-absorbed	1.5	0.03	1.5	50.0
$2\,LiH + MgB_2 + 0{\cdot}1\,Zr-$iso-desorbed	0.8	0.03	0.8	26.7
$2\,LiH + MgB_2 + 0{\cdot}1\,VCl_3$-absorbed	2.0	0.03	2.1	40.0
$2\,LiH + MgB_2 + 0{\cdot}1\,VCl_3$-desorbed	2.4	0.03	2.5	60.0
$2\,LiH + MgB_2 + 0{\cdot}1\,VCl_3$-milled	2.0	0.03	2.1	40.0

The fitting results reveal similar characteristic lengths of 1-2.5 nm for V-based additives. Besides the fitting, the slope of the scattering cross section contains information on the shape of the structures. Proportionalities to q^{-3} and $q^{-2.5}$ were estimated for composites with Zr-based additives and V-based additives, respectively. This is an indication for mass fractals or polydispesity and especially for the V-

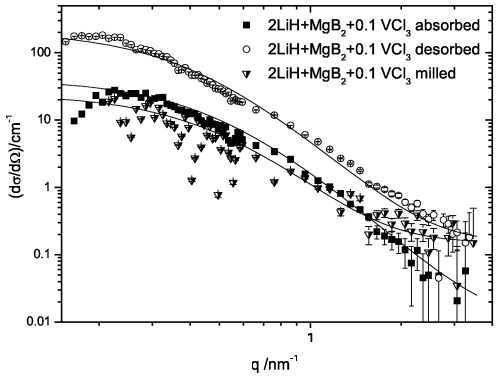

Figure 6. Separated scattering curves for $2\,\mathrm{LiH} + \mathrm{MgB_2}$ +0.1 $\mathrm{VCl_3}$ composites in the milled, absorbed and desorbed state obtained from ASAXS measurements at the K-absorption edge of V at 5465 eV.

compounds a formation of slightly anisotropic structures is likely.

In figure 7, the separated scattering curves for the sample $2\,\mathrm{LiBH_4} + \mathrm{MgH_2}$ +0.1 Zr-iso-absorbed and the distance distribution function fitted using the GNOM program [28] is shown. The distance distribution shows the probability of distances between scattering centers in the sample and gives an estimate of the maximum sizes, which are present in the sample. Figure 7(b) shows exemplarily the width of the distance distribution of the Zr-containing structures with maximum length of about 4 nm and a maximum around 2 nm, which is in good agreement with the previously determined correlation length; see table 2. For this fit, the scattering from larger inhomogeneities at low q values was neglected. Similar distance distributions were obtained for all samples.

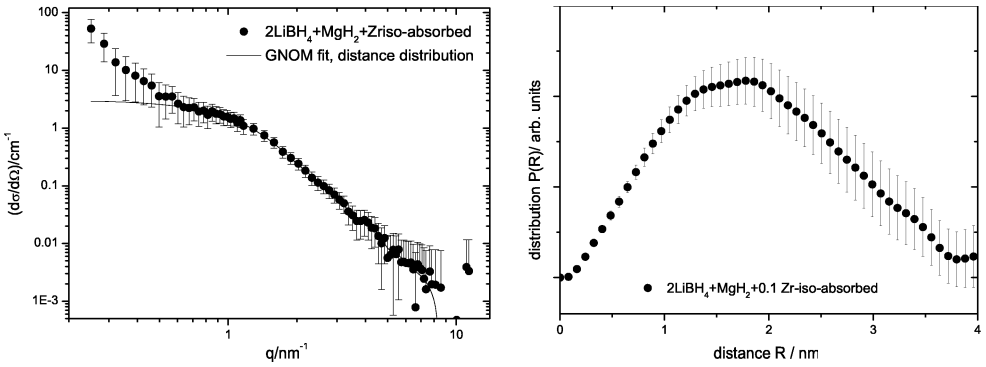

(a) Separated scattering curve (b) obtained distance distribution

Figure 7. Separated scattering curve for $2\,\mathrm{LiBH_4} + \mathrm{MgH_2}$ +0.1 Zr-iso-absorbed composites obtained from ASAXS measurements at the K-absorption edge of Zr at 17998 eV and the corresponding distance distribution using the GNOM program.

4. Discussion

The results obtained in this study show that in all the investigated cases the transition metal based additives (VCl_3, $ZrCl_4$, Zr-iso) show a very fine distribution, either already after milling or after the first sorption reactions. For the Zr-based additives, the formation of stable ZrB_2 is proposed; for V-based additives a similar XANES study is currently performed. An average precipitation size of the transition-metal compounds of 1 to 2 nm was determined by fitting a correlation length model.

In comparison with the literature for TiB_2 precipitations in MgB_2 by doping with Ti, a distribution of very fine nanoparticles in the grain boundaries as well as in the matrix was observed by TEM investigations [29; 30]. A segregation of the precipitates in the grain boundaries may be reasonable, because the sorption reactions involve complex phase transformation with significant mass transport. The precipitates could be swept into the grain boundaries and prevent coarsening by stabilization of the grain boundaries. This is supported by the fact that from the crystallite sizes, assessed for the Mg-phases by applying the Scherrer equation, no significant coarsening can be observed after the sorption processes (data not shown). A formation of a network of the Zr- or V- based compounds in the grain boundaries could also lead to the observed scattering from larger structures observed at low q values. In all cases with Zr- or V-based additives, a significant enhancement of the reaction kinetics could be observed in volumetric measurements. In particular, the reduction of the incubation period between the two desorption steps is striking. In an earlier study, a nucleation problem of MgB_2 was proposed to be the origin of the incubation period [8]. Calculations have shown, that the lattice misfits, which are important factors for heterogeneous nucleation, are rather small for MgB_2 on ZrB_2 or VB_2 because the three phases have the same hexagonal lattice structure. Therefore the observed ZrB_2 might act as a nucleation agent for MgB_2. Furthermore, borides especially TiB_2 are known as outstanding grain refiners in Mg- and Al-alloys [31; 32]. Recently, *in-situ* neutron diffraction study by Singh *et al* [33] on $NaAlH_4$ supports the correlation of small grains and sites for heterogeneous nucleation with the catalyst. They have observed a significant grain coarsening for uncatalysed $NaAlH_4$ while for the samples with $TiCl_3$ catalysed $NaAlH_4$ the grain size remained small during the sorption reactions.

However, the different reaction rates obtained for the two additives $ZrCl_4$ and Zr-iso indicate that this is probably not the only explanation. Already in a simple binary light weight hydride system like MgH_2, the function of transition metal compound additives and especially transition metal oxides is rather complex. According to Dornheim *et al* [34] transition metal oxides do not only accelerate surface reaction kinetics by catalytic effect but also have a clear influence on the MgH_2 particle size during milling as well as the stabilization of crystallite sizes during cycling at elevated temperatures. Zhou [35] modeled the kinetics of LiH - MgB_2 composites with different transition metal additives based on a series of volumetric measurements. According to the different shapes of the respective absorption and desorption curves they concluded that the use of different

additives leads to different rate limiting steps for the reactions of the RHC. This indicates that the effect of the additives on the reaction mechanism in the composites is rather complex and that there will be no single explanation for the different additives and their effect on the reaction kinetics.

In literature no study was found which would support a potential catalytic activity of the ZrB_2 for hydrogen splitting or recombination. For example, early measurements by Lavrenko *et al* [36] and Samsonov and Kharmalov [37] revealed a rather low activity of ZrB_2 with respect to hydrogen. This is related to the charge-free surfaces. In any case, a catalytic effect of ZrB_2 on the hydrogen reaction should lead to similar sorption rates since ZrB_2 is formed in both investigated cases, and the size and distribution are similar.

As indicated by this discussion, numerous origins for the reaction enhancement with additional transition metal additives are possible. A combination of multiple effects may therefore also be likely.

5. Conclusions

Transition metal based additives have a significant influence on the sorption kinetics of reactive hydride composites such as $2\,LiBH_4$ - MgH_2 composites. In the present study, the chemical state and the microstructural distribution of the Zr- and V-based additives, $ZrCl_4$, Zr-isopropoxide isopropanol complex and VCl_3 were investigated by means of XANES and ASAXS. For the first time the chemical state and distribution of the transition metal compound formed by these additives for reactive hydride composites has been experimentally determined by use of XANES/ASAXS. The formation of ZrB_2 or V-based nanoparticles with a typical length-scale of 1-2 nm is proposed for Zr- or V-based additives. How these nanoparticles influence the reaction kinetics in detail remains unclear and is subject of further studies.

Acknowledgments

Partial funding by the Helmholtz Initiative 'Functional Materials for Mobile Hydrogen Storagey' is gratefully acknowledged by the authors.

References

[1] Libowitz G, Hayes H and Gibb T 1958 *J. Phys. Chem.* **62** 76

[2] Reilly J and Wiswall R 1967 *Inorg. Chem.* **6** 2220–2223

[3] Reilly J J and Wiswall R H 1968 *Inorg. Chem.* **7** 2254–2256

[4] Barkhordarian G, Klassen T and Bormann R , priority 2004, Patent pending, German Pub. No: DE102004/061286

[5] Barkhordarian G, Klassen T, Dornheim M and Bormann R 2007 *J. Alloys Compounds* **440** L18–L21

[6] Vajo J J, Mertens F, Skeith S and Balogh M , priority 2004, Patent pending, Int. Pub. No: WO 2005/097671 A2

[7] Vajo J J, Skeith S L and Mertens F 2005 *J. Phys. Chem. B* **109** 3719–3722

[8] Bösenberg U, Doppiu S, Mosegaard L, Barkhordarian G, Eigen N, Borgschulte A, Jensen T R, Cerenius Y, Gutfleisch O, Klassen T, Dornheim M and Bormann R 2007 *Acta Mater.* **55** 3951–3958

[9] Nakagawa T, Ichikawa T, Hanada N, Kojima Y and Fujii H 2007 *J. Alloys Compounds* **446-447** 306–309

[10] Vajo J J, Mertens F, Ahn C C, Bowman R C and Fultz B 2004 *J. Phys. Chem. B* **108** 13977–13983

[11] Pinkerton F E, Meyer M S, Meisner G P, Balogh M P and Vajo J J 2007 *J..Phys. Chem. C* **111 (35)** 12881 –12885

[12] Bogdanovic B and Schwickardi M 1997 *J. Alloys Compounds* **253-254** 1–9

[13] Oelerich W, Klassen T and Bormann R 2001 *J. Alloys Compounds* **315** 237–242

[14] Deprez E 2008 Master's thesis University of Sevilla

[15] Stuhrmann H, Goerigk G and Munk B 1991 *Handbook on Synchrotron Radiation* (Elsevier Science Publishers) chap 17, Anomalous X-ray Scattering, pp 555–580

[16] Attenkofer K 2000 *Die magnetische Kopplung in ausgewählten Verbindungen - Neue Möglichkeiten und Entwicklungen der Rumpfanregungspektroskopie mit zirkularpolarisierten Photonen* Ph.D. thesis Hamburg

[17] Attenkofer K, Tröger L, Herrmann M and Brüggmann U 1998 HASYLAB Annual Report 1998

[18] Haubold H G, Gruenhagen K, Wagener M, Jungbluth H, Heer H, Pfeil A, Rongen H, Brandenberg G, Moeller R, Matzerath J, Hiller P and Halling H 1989 *Rev. Sci. Instrum.* **60** 1943–1946

[19] Goerigk G 2006 Electronic and Computer Upgrade at ASAXS Beamline JUSIFA HASYLAB Annual Report 2006

[20] Fuoss P H, Eisenberger P, Warburton W K and Bienenstock A 1981 *Phys. Rev. Lett.* **46** 1537–1540

[21] Vainio U, Pirkkalainen K, Kisko K, Goerigk G, Kotelnikova N and Serimaa R 2007 *Eur. Phys. J. D* **42** 92–101

[22] Evans G and Pettifer R 2001 *J. Appl. Crystallogr.* **34** 82–86

[23] Evans G 2004 *CHOOCH, Manual, Determination of Anomalous Scattering Factors from X-ray fluorescence data*

[24] Kraft S, Stümpel J, Becker P and Kuetgens U 1996 *Rev. Sci. Instrum.* **67** 681–687

[25] Debye P, Anderson H J and Brumberger H 1957 *J. Appl. Phys.* **28, No. 6** 679–683

[26] Goerigk G and Williamson D L 1998 *Solid State Commun.* **108, No. 7** 419–424

[27] Goerigk G and Williamson D L 2001 *J. Non-Cryst. Solids* **281** 181–188

[28] Svergun D and Semenyuk A 2003 PROGRAM PACKAGE GNOM http://www.embl-hamburg.de/ExternalInfo/Research/Sax/

[29] Zhao Y, Feng Y, Cheng C, Zhou L, Wu Y, Machi T, Fudamoto Y, Koshizuka N and Murakam M 2001 *Appl. Phys. Lett.* **79** 1154

[30] Kramer M, Bud'ko S L, Canfield P, Wilke R, Finnemore D and Raymond J 2007 *cond-mat. supr-con* **arXiv:condmat/0302443v1**

[31] Wang Y, Wang H, Yang Y and Jiang Q 2008 *Mater.Sci. Eng. A* **478** 9–15

[32] Qiu D, Zhang M X, Fu H M, Kelly P and Taylor J 2007 *Phil. Mag. Lett.* **87** 505–514

[33] Singh S, Eijt S, Huot J, Kockelmann W, Wagemaker M and Mulder F 2007 *Acta Mater.* **55** 5549–5557

[34] Dornheim M, Eigen N, Barkhordarian G, Klassen T and Bormann R 2006 *Adv. Eng. Mater.* **5** 377–385

[35] Zhou Y 2007 Master's thesis Technical University of Hamburg-Harburg

[36] Lavrenko V, Vasil'ev A and Rokhlenko A 1974 *Theor. Exp. Chem.* **7 No. 5** 564–567

[37] Samsonov G and Kharlamov A 1976 *Powder Metall. Met. Ceram.* **14, No. 9** 699–707